Quantum Nature of the Proton in Water-Hydroxyl Overlayers on Metal Surfaces

Xin-Zheng Li,[1] Matthew I. J. Probert,[2] Ali Alavi,[3] and Angelos Michaelides[1,*]

[1]*London Centre for Nanotechnology and Department of Chemistry, University College London, London WC1E 6BT, United Kindgom*
[2]*Department of Physics, University of York, York YO10 5DD, United Kingdom*
[3]*Department of Chemistry, University of Cambridge, Lensfield Road, Cambridge CB2 1EW, United Kingdom*

(Received 29 September 2009; published 11 February 2010)

Using *ab initio* path-integral molecular dynamics, we show that water-hydroxyl overlayers on transition metal surfaces exhibit surprisingly pronounced quantum nuclear effects. The metal substrates serve to reduce the classical proton transfer barriers within the overlayers and, in analogy to ice under high pressure, to shorten the corresponding intermolecular hydrogen bonds. Depending on the substrate and the intermolecular separations it imposes, the traditional distinction between covalent and hydrogen bonds is lost partially [e.g., on Pt(111) and Ru(0001)] or almost entirely [e.g., on Ni(111)]. We suggest that these systems provide an excellent platform on which to systematically explore the magnitude of quantum nuclear effects in hydrogen bonds.

DOI: 10.1103/PhysRevLett.104.066102 PACS numbers: 68.43.Bc, 71.15.Pd, 82.45.Jn, 82.65.+r

Under ambient conditions, most surfaces are covered in a film of water [1]. As such, wet surfaces are of pervasive importance in processes like corrosion, friction, and ice nucleation. On many surfaces, the first contact layer of water is not comprised of pure water but instead of a mixture of water and hydroxyl molecules [1–11]. These overlayers form because they offer the optimal balance of hydrogen (H) bonding within the overlayer and bonding to the surface, and they have now been observed on several oxide, semiconductor, and metal surfaces.

Water-hydroxyl wetting layers are most well characterized on close-packed metal surfaces under ultrahigh vacuum (UHV) conditions [1]. The molecules in the overlayer are typically ''pinned'' in registry with the substrate, bonding above individual metal atoms in H bonded networks (see Fig. 1). As a consequence, the distance between adjacent molecules is dictated by the substrate, being relatively large on a metal with a large lattice constant [e.g., ~2.83 Å on average on Pt(111)] and much smaller on a metal with a relatively small lattice constant [e.g., ~2.50 Å on average on Ni(111)]. It is known from studies of water in other environments, e.g., certain phases of bulk ice, that the nature of the shared proton in intermolecular H bonds varies dramatically over such a large range of O-O distances. Specifically, under ambient pressures bulk ice is a conventional molecular crystal, with O-O separations of ~2.8 Å. However, at very high pressure (≥ 70 GPa), with O-O separations of ~2.3 Å, ice loses its integrity as a molecular crystal and the protons become delocalized between the O nuclei (see, e.g., [12–14]).

The correspondence with ice under pressure suggests that water-hydroxyl overlayers may exhibit pronounced substrate dependent quantum nuclear effects. Although this possibility has not been discussed until now, recent experiments for closely related systems, namely, water clusters on metal surfaces, indicate that quantum effects can be important. Specifically, quantum tunneling has been suggested to explain the anomalously rapid diffusion and H bond dynamics of water clusters on Pd and Cu [15,16]. To tackle the water-hydroxyl overlayers, we performed *ab initio* path-integral molecular dynamics (PIMD) simulations on Pt(111), Ru(0001), and Ni(111) at 160 K, a typical temperature used in experimental studies of these systems. In *ab initio* PIMD, both the electrons and nuclei are treated as quantum particles in contrast to traditional *ab initio* molecular dynamics (MD) in which the nuclei are classical pointlike particles and only the electrons are treated quantum mechanically (see, e.g., [12,17–19]). All

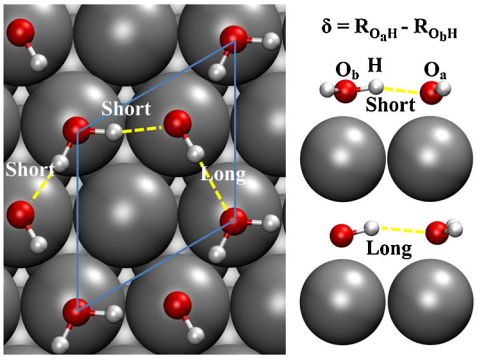

FIG. 1 (color online). Structure of the $\sqrt{3} \times \sqrt{3} - R30°$ overlayer (with classical nuclei) that forms on metal surfaces. Side views when the proton is donated from water to hydroxyl (upper, labeled ''short'') and from hydroxyl to water (lower, labeled ''long'') are shown on the right. Classically, at the ground state, the short and long H bond lengths are ~1.7 and ~2.1 Å on Pt, ~1.6 and ~1.9 Å on Ru, and ~1.4 and ~1.6 Å on Ni, respectively. The coordinate for proton transfer δ is defined as $R_{O_aH} - R_{O_bH}$, where R_{O_aH} and R_{O_bH} are the instantaneous O-H distances between O_a and H and O_b and H, respectively. For a proton equidistant from its two O neighbors $\delta = 0$ and upon transfer from one O to another δ changes sign.

calculations were performed using the plane-wave density-functional theory (DFT) code CASTEP [20] with the Perdew-Burke-Ernzerhof (PBE) exchange-correlation functional [21] and $\sqrt{3} \times \sqrt{3} - R30°$ surface unit cells [22]. Pt and Ru were selected because they support well-characterized $\sqrt{3} \times \sqrt{3} - R30°$ water-hydroxyl overlayers (see, e.g., Refs. [1–7,23–25]) and Ni because it has a relatively small lattice constant, although water-hydroxyl films have not yet been characterized on it [1].

The simulations reported here reveal that when quantum nuclear fluctuations are taken into account, the distinction between covalent and H bonds lessens considerably [on Pt(111) and Ru(0001)] or almost completely disappears [on Ni(111)], and as a consequence the traditional "ball-and-stick" description of the molecules in the overlayers is no longer appropriate. In addition, the quantum fluctuations can impact indirectly on the O atom positions within the overlayer, altering the relative proportion of short and long O-O distances. Overall, this study reveals that water-hydroxyl overlayers on metal surfaces exhibit pronounced quantum nuclear effects and that there is a subtle interplay between the quantum nature of the proton in these overlayers and the lattice constant of the substrate. This interplay suggests that water-metal interfaces provide an excellent platform on which to systematically tune the magnitude of quantum effects in H bonds.

Before we consider these systems at a quantum level, we briefly look at their properties in the classical perspective. The overlayers are comprised of hexagonal H bonded networks of water and hydroxyl bonded above metal atoms of the substrate in a $\sqrt{3} \times \sqrt{3} - R30°$ periodicity. Both types of molecule lie almost parallel to the surface, forming an extended 2D network. Because OH is a better acceptor of H bonds than it is a donor, there is an asymmetry in the overlayer with each molecule involved in two short and one long H bond at the classical ground state (Fig. 1). At finite temperature, *ab initio* MD simulations with classical nuclei show that this asymmetry is still present, although thermal broadening causes the peaks associated with the long and short H bonds to overlap, particularly on Ni which has the smallest lattice constant. The asymmetry is illustrated in Fig. 2 where probability distributions of O-H and O-O distances are plotted on Pt, Ru, and Ni. In addition, the probability distributions of O-H distances clearly show that the overlayer in the classical picture is comprised of individual H_2O and OH molecules H bonded to each other. There is a sharp peak at ~1.0 Å characteristic of the covalent bonds of water and hydroxyl and broader peaks at ~1.7–2.1 Å, ~1.6–1.9 Å, and ~1.5 Å characteristic of the H bonds on Pt, Ru, and Ni, respectively.

Let us now consider how the picture that emerges differs at the quantum mechanical level with PIMD. A key result is that there is no longer a clear division between short covalent and longer H bonds. This is clear from the distributions of O-H and O-O distances plotted alongside the classical results in Fig. 2 (in the PIMD simulations, distances are measured between the centroids of each quantum particle; results obtained by measuring the average bead distances are the same). Looking at Pt first, the population of covalent O-H bonds is reduced by one third and replaced with a clearly nonzero probability distribution over the entire range of 1–1.5 Å [Fig. 2(a)]. Likewise, the proportion of short O-O distances is reduced from two thirds to one third, and the center of the peak associated with the short O-O separations moves from ~2.7 to ~2.5 Å [Fig. 2(b)]. These changes are associated with one third of the shared protons being delocalized between the two Os to which they are bonded. This delocalized proton, in turn, "pulls" the Os closer together and in so doing creates an "H_3O_2 complex" with a shared proton that is neither well described as being covalently nor H bonded to its two Os. A typical snapshot from the PIMD simulation is shown in Fig. 2(g) with the H_3O_2 complex located along one particular O-O axis. The snapshot also shows how when the two Os on either side of the shared proton are drawn together, the distances to their other O neighbors are increased. It is this effect that leads to a

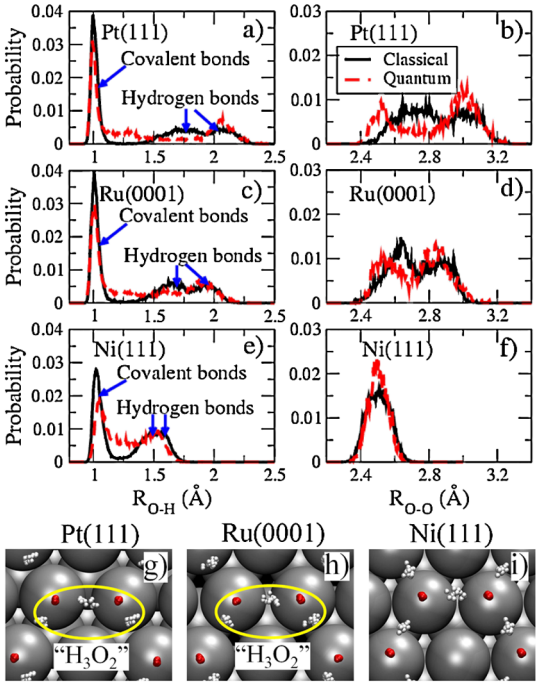

FIG. 2 (color online). Selected structural properties of the classical and quantum overlayers. Probability distributions of O-H [(a), (c), (e)] and O-O distances [(b), (d), (f)] on Pt, Ru, and Ni at 160 K, as obtained from MD with classical nuclei (labeled classical, black solid lines) and PIMD [labeled quantum, (red) dashed lines]. On the bottom [(g)–(i)] snapshots for typical spatial configurations of the overlayer on Pt (left), Ru (middle), and Ni (right) obtained from PIMD (with every atom represented by 16 beads) are shown. On Pt and Ru at any given snapshot one proton is equally shared by two of the Os yielding an intermediate "H_3O_2" complex. On Ni at any given snapshot several protons can simultaneously be shared between the oxygens.

larger proportion of long O-O distances than was observed in the classical picture [Fig. 2(b)]. On Ru, similar delocalization of the H atoms is observed and again the structure contains a H_3O_2 complex [Fig. 2(h)]. The smaller lattice constant of Ru means that only a small enhancement in the proportion of short O-O separations (at ~2.5 Å) is required to enable proton delocalization [Fig. 2(d)]. Upon moving to Ni, the effects brought about through quantum fluctuations of the protons are even more pronounced [Fig. 2(e)], and the peaks associated with the covalent O-H bonds are broadened so much that a broad double peaked distribution emerges, totally eliminating the distinction between covalent and H bonds in the classical picture. Because of the smaller lattice constant of Ni, this delocalization is possible without any major rearrangement of the O atom "skeleton" [Fig. 2(f)] and, as a consequence, several protons can be simultaneously delocalized. A snapshot from the PIMD simulations on Ni in which several protons are delocalized and the distinction between covalent and H bonds is completely lost is shown in Fig. 2(i).

The different probability distributions observed in the classical and quantum simulations reveal the fundamentally different nature of the two. To examine this from a more rigorous statistical perspective, we now consider the free energy profiles for the protons along the intermolecular axes (Fig. 3). We define the coordinate for proton transfer δ as the difference between two instantaneous O-H distances (see the caption of Fig. 1 for details). For the analysis to be as unbiased as possible, all inequivalent H bonds in the system are taken into account, i.e., the free energy profile discussed at this stage is an average over all H bonds in the overlayer. The profile from the MD simulations with classical nuclei is characterized by two partially overlapping valleys corresponding to the short and long H bonds at $\delta \sim 0.7$ and $\delta \sim 1.1$ Å on Pt and $\delta \sim 0.6$ and $\delta \sim 0.9$ Å on Ru. On Ni, a single broad valley at $\delta \sim 0.5$ Å is observed, since, as we have said, thermal broadening obscures the distinction between short and long H bonds on this surface. In the classical simulations, thermally activated proton transfer is infrequent, consistent with the presence of relatively large classical free energy barriers on all three substrates at $\delta = 0$. Moving to the quantum free energy profiles obtained from the PIMD simulations, it can be seen that they differ significantly from the classical profiles. On both Pt and Ru the minima for the long H bonds remain, but those associated with the short H bonds disappear due to the formation of the intermediate H_3O_2 complexes discussed already. On Ni, the single valley at $\delta \sim 0.5$ Å is softened and shifted to $\delta \sim 0.4$ Å. The key differences, however, between the quantum and classical free energy profiles is that the quantum free energy barriers are considerably smaller than the classical ones. In addition, upon going from Pt to Ru to Ni, the height of the barrier and the area beneath it decreases. This indicates that the proton transfer probability increases as the lattice constant is reduced.

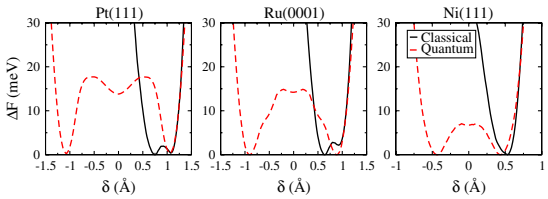

FIG. 3 (color online). Free energy profiles (ΔF) for the protons along the intermolecular axes on Pt (left), Ru (middle), and Ni (right) at 160 K, obtained from MD (labeled classical, black solid lines) and PIMD [labeled quantum, (red) dashed lines]. The reaction coordinate δ is defined in Fig. 1. The free energy is calculated from $\Delta F(\delta) = -k_B T \ln[P(\delta)]$, where $P(\delta)$ is the probability distribution of δ and k_B is the Boltzmann constant.

So far we have seen evidence for a connection between proton delocalization and the O-O distance distributions, as illustrated in Figs. 2(b) and 2(d) for Pt and Ru, respectively. A deeper understanding of this behavior can be obtained by correlating the location of the proton along the intermolecular axes with the corresponding O-O distances. To this end, in Fig. 4, probability distribution functions of δ and $R_{O\text{-}O}$ are plotted from the MD and PIMD simulations. In the classical perspective [Figs. 4(a), 4(d), and 4(g)], these are characterized by negligible probability distributions at $\delta = 0$, consistent with the fact that each proton covalently bonds to one O and hops from one side to the other over a barrier at $\delta = 0$. The O-O distribution has peaks for the

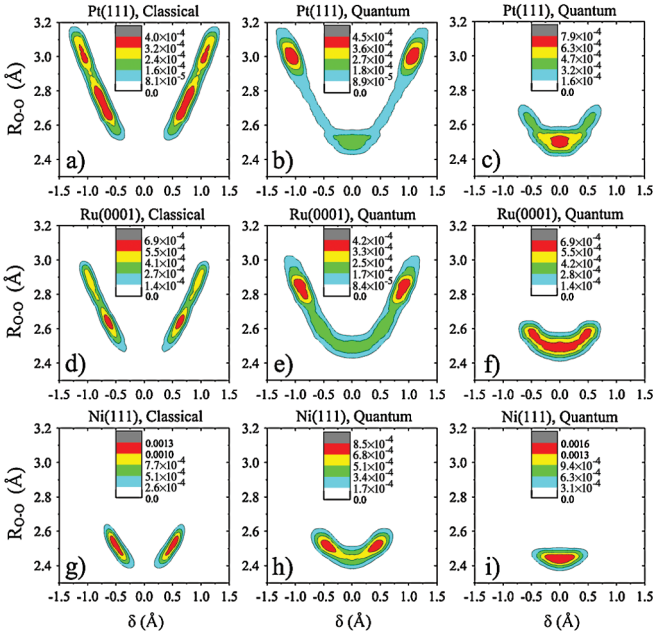

FIG. 4 (color). Probability distributions in the MD [(a), (d), (g)] and PIMD [(b), (e), (h)] simulations as functions of δ and R_{OO}. δ is the reaction coordinate as defined in Fig. 1. In panels (c), (f), and (i) probability distribution functions for only the "most active proton," that is, the proton with smallest δ at each time step, are shown. All MD and PIMD distribution functions have been symmetrized about δ. For more details on the simulation lengths, see the supplementary information in Ref. [22].

short and long H bonds on Pt and Ru and one merged peak on Ni. When quantum fluctuations are included, finite distributions at $\delta = 0$ appear on all three substrates. These correspond to the delocalized protons, and the associated O-O distance of these protons is $\sim$2.4– $\sim$ 2.5 Å on each substrate. To understand the delocalized protons in more detail, we now focus on the proton which at any given snapshot in the PIMD simulations has the smallest δ. This is the so-called ''most active proton,'' the one that has the greatest likelihood of transferring [19]. On Pt and Ru, this is the proton located within the shortest O-O bond. On Ni, where the average O-O distance is $\sim$2.5 Å, the most active proton need not necessarily be the one within the shortest O-O bond. The results of this analysis are reported in Figs. 4(c), 4(f), and 4(i), with the key finding being that on all substrates the probability distributions for the most active proton exhibit a single maximum at $\delta = 0$. Therefore, the corresponding free energy barrier for the transfer of this most active proton is zero and the classical barrier is wiped out by quantum fluctuations. The ''horseshoe'' shape of the probability distributions on Pt and Ru reveal that the covalently bonded proton requires the O atoms to at first move together before the proton becomes delocalized between the two oxygens. At this point, the zero point energy level of the proton resides above the classical potential energy barrier. Subsequent thermal fluctuations cause the oxygens to move apart and, in so doing, the proton can be transferred from one O to the other. Therefore, the mechanism for proton transfer on Pt and Ru is the so-called ''adiabatic proton transfer'' [26], predicted for the diffusion mechanism of the excess proton in water and for ice at certain pressures [12,19]. For the excess proton in water and ice, it is electrostatics and pressure, respectively, that enable proton transfer whereas here it is the substrate. On Ni, due to the small lattice constant, the O-O distances are already short enough such that proton delocalization is possible without rearrangement of the O atoms.

The results reported here demonstrate that quantum delocalization has a profound impact on water-hydroxyl overlayers on Pt, Ru, and Ni, leading to a blurring of the lines between covalent and H bonds. We expect that equally pronounced quantum behavior will be observed for similar overlayers on other metal substrates, especially those which have relevant interatomic distances between those of Ni and Pt. More generally these effects will be relevant to many other interfacial and confined water systems including biological and aqueous systems whenever the substrate forces the molecules close together or polarizes them so as to reduce the proton transfer barriers. The impact the quantum nature of the shared proton can have on the heavy atom O skeleton suggests that a quantitative low-energy electron diffraction analysis, on, e.g., Pt, prepared with light and heavy water may provide a means to experimentally verify some of the predictions made here. Similarly, signatures of the quantum delocalization for interfacial water may be detectable with techniques such as electron energy loss spectroscopy, scanning tunneling microscopy, helium scattering, or neutron Compton scattering. We hope this work will stimulate such studies.

This work was supported by the European Research Council, the EURYI scheme, and the EPSRC. We are grateful to UCL Research Computing and HECTOR (the UK's national high-performance computing service) for computational resources.

Note added in proof.—Experimental support for proton delocalization in a single water-hydroxyl dimer on Cu(110) has recently been observed with scanning tunneling microscopy [27].

*angelos.michaelides@ucl.ac.uk

[1] A. Hodgson and S. Haq, Surf. Sci. Rep. **64**, 381 (2009).
[2] G. Held and D. Menzel, Surf. Sci. **316**, 92 (1994).
[3] A. Michaelides and P. Hu, J. Am. Chem. Soc. **123**, 4235 (2001).
[4] P. J. Feibelman, Science **295**, 99 (2002).
[5] S. Völkening *et al.*, Phys. Rev. Lett. **83**, 2672 (1999).
[6] C. Clay, S. Haq, and A. Hodgson, Phys. Rev. Lett. **92**, 046102 (2004).
[7] T. Schiros *et al.*, J. Phys. Chem. C **111**, 15 003 (2007).
[8] L. Giordano, J. Goniakowski, and J. Suzanne, Phys. Rev. Lett. **81**, 1271 (1998).
[9] Y. D. Kim *et al.*, Chem. Phys. Lett. **352**, 318 (2002).
[10] B. Meyer *et al.*, Angew. Chem., Int. Ed. **43**, 6641 (2004).
[11] A. Michaelides, A. Alavi, and D. A. King, Phys. Rev. B **69**, 113404 (2004).
[12] M. Benoit, D. Marx, and M. Parrinello, Nature (London) **392**, 258 (1998).
[13] E. Schwegler *et al.*, Proc. Natl. Acad. Sci. U.S.A. **105**, 14 779 (2008).
[14] J. A. Morrone, L. Lin, and R. Car, J. Chem. Phys. **130**, 204511 (2009).
[15] V. A. Ranea *et al.*, Phys. Rev. Lett. **92**, 136104 (2004).
[16] T. Kumagai *et al.*, Phys. Rev. Lett. **100**, 166101 (2008).
[17] D. Marx and M. Parrinello, J. Chem. Phys. **104**, 4077 (1996).
[18] M. E. Tuckerman *et al.*, Science **275**, 817 (1997).
[19] D. Marx *et al.*, Nature (London) **397**, 601 (1999).
[20] S. J. Clark *et al.*, Z. Kristallogr. **220**, 567 (2005).
[21] J. P. Perdew, K. Burke, and M. Ernzerhof, Phys. Rev. Lett. **77**, 3865 (1996).
[22] See supplementary material at http://link.aps.org/supplemental/10.1103/PhysRevLett.104.066102 for details of the computational setups, additional results, and convergence tests, including results on Pt for a $2\sqrt{3} \times 2\sqrt{3} - R30°$ cell, which show that the qualitative features observed in the $\sqrt{3} \times \sqrt{3} - R30°$ persist when a much larger cell is used.
[23] C. Sachs *et al.*, Science **293**, 1635 (2001).
[24] G. Held *et al.*, J. Chem. Phys. **123**, 064711 (2005).
[25] N. S. Faradzhev *et al.*, Chem. Phys. Lett. **415**, 165 (2005).
[26] K. Ando and J. T. Hynes, J. Phys. Chem. B **101**, 10 464 (1997).
[27] T. Kumagai *et al.*, Phys. Rev. B **81**, 045402 (2010).